PAPER

# Maximization of ICRF power by SOL density tailoring with local gas injection

To cite this article: P. Jacquet *et al* 2016 *Nucl. Fusion* **56** 046001

IOP Publishing | International Atomic Energy Agency Nuclear Fusion

Nucl. Fusion **56** (2016) 046001 (14pp) doi:10.1088/0029-5515/56/4/046001

# Maximization of ICRF power by SOL density tailoring with local gas injection

**P. Jacquet[1], M. Goniche[2], V. Bobkov[3], E. Lerche[4,1], R.I. Pinsker[5], R.A. Pitts[6], W. Zhang[3,7], L. Colas[2], J. Hosea[8], S. Moriyama[9], S.-J. Wang[10], S. Wukitch[11], X. Zhang[12], R. Bilato[3], H. Bufferand[2], L. Guimarais[13], H. Faugel[3], G.R. Hanson[14], M. Kocan[6], I. Monakhov[1], J.-M. Noterdaeme[3,7], V. Petrzilka[15], A. Shaw[1], I. Stepanov[3,7], A.C.C. Sips[16], D. Van Eester[4], T. Wauters[4], the JET contributors[17,18] and the ASDEX Upgrade team, the DIII-D team and the ITPA 'Integrated Operation Scenarios' members and experts**

[1] CCFE, Culham Science Centre, Abingdon, OX14 3DB, UK.
[2] CEA, IRFM, F-13108 Saint-Paul-Lez-Durance, France.
[3] Max-Planck-Institut für Plasmaphysik, Garching, Germany.
[4] LPP-ERM/KMS, EUROfusion Consortium Member - Trilateral Euregio Cluster, Brussels, Belgium
[5] General Atomics, PO Box 85608, San Diego, CA 92186–5608, USA
[6] ITER Organization, Route de Vinon-sur-Verdon, CS 90 046, 13067 St. Paul Lez Durance Cedex, France
[7] Applied Physics Department, UGent, Gent, Belgium
[8] Princeton Plasma Physics Laboratory, Princeton, NJ 08543, USA
[9] Japan Atomic Energy Agency, 801-1, Mukouyama, Naka, Ibaraki-ken 311-0193, Japan
[10] National Fusion Research Institute, Yuseong, Daejeon, 305–806, Korea
[11] MIT Plasma Science and Fusion Center, Cambridge, MA 02139, USA
[12] Institute of Plasma Physics, Chinese Academy of Sciences, Hefei 230031, People's Republic of China
[13] Instituto de Plasmas e Fusão Nuclear, IST, Universidade de Lisboa, Portugal
[14] Oak Ridge National Laboratory, Oak Ridge, TN 37831, USA
[15] IPP.CR, Za Slovankou 3, 182 21 Praha 8, Czech Republic
[16] European Commission, B1049 Brussels, Belgium
[17] EUROfusion Consortium, JET, Culham Science Centre, Abingdon, OX14 3DB, UK

E-mail: philippe.jacquet@ukaea.uk

Received 17 August 2015, revised 29 December 2015
Accepted for publication 11 January 2016
Published 2 March 2016


**Abstract**

Experiments have been performed under the coordination of the International Tokamak Physics Activity (ITPA) on several tokamaks, including ASDEX Upgrade (AUG), JET and DIII-D, to characterize the increased Ion cyclotron range of frequency (ICRF) antenna loading achieved by optimizing the position of gas injection relative to the RF antennas. On DIII-D, AUG and JET (with the ITER-Like Wall) a 50% increase in the antenna loading was observed when injecting deuterium in ELMy H-mode plasmas using mid-plane inlets close to the powered antennas instead of divertor injection and, with smaller improvement when using gas inlets located at the top of the machine. The gas injection rate required for such improvements (~$0.7 \times 10^{22}$ el $s^{-1}$ in AUG, ~$1.0 \times 10^{22}$ el $s^{-1}$ in JET) is compatible with the use of this technique to optimize ICRF heating during the development of plasma scenarios and no degradation of confinement was observed when using the mid-plane or top inlets compared with divertor valves. An increase in the scrape-off layer (SOL) density was measured when switching gas injection from divertor to outer mid-plane or top. On JET and DIII-D, the measured SOL density increase when using main chamber puffing is consistent with the antenna coupling resistance increase provided that the distance between the measurement lines of sight and the injection location is taken into account. Optimized gas injection was also

[18] See the appendix of [54].

 

found to be beneficial for reducing tungsten (W) sputtering at the AUG antenna limiters, and also to reduce slightly the W and nickel (Ni) content in JET plasmas. Modeling the specific effects of divertor/top/mid-plane injection on the outer mid-plane density was carried out using both the EDGE2D-EIRENE and EMC3-EIRENE plasma boundary code packages; simulations indeed indicate that outer mid-plane gas injection maximizes the density in the mid-plane close to the injection point with qualitative agreement with the AUG SOL density measurements for EMC3-EIRENE. Field line tracing for ITER in the 15 MA $Q_{DT} = 10$ reference scenario indicates that the planned gas injection system could be used to tailor the density in front the antennas. Benchmarking of EMC3-EIRENE against AUG and JET data is planned as a first step towards the ITER SOL modelling required to quantify the effect of gas injection on the SOL density in front of the antennas.

Keywords: ICRF power, antenna loading, gas injection, SOL density

(Some figures may appear in colour only in the online journal)

## 1. Introduction

Ion cyclotron range of frequency (ICRF) wave heating of tokamak plasmas relies on the propagation and the absorption of the fast wave, which is evanescent until it reaches a plasma density which exceeds the cut-off value $n_{e\_CutOff}$ [1]. For the ICRF frequencies used to heat tokamak plasmas (~30–100 MHz) and fast wave toroidal numbers ($k_{//}$ in the range 3–10 $m^{-1}$) $n_{e\_CutOff}$ is in the $10^{18}$ $m^{-3}$ range, which is typical of the scrape-off Layer (SOL) density. The ICRF power coupled to the plasma from the antenna can be expressed as:

$$P_{coupled} \sim V_{max}^2 R_c / 2Z_c^2 \quad (1)$$

where $R_c$ is the antenna coupling resistance. The antenna is fed by transmission lines with characteristic impedance $Z_c$, and $V_{max}$ is the anti-node voltage in the transmission line. In practice on many tokamaks, the ICRF power coupled to the plasma is limited by the increased risk of arcing in the transmission lines when $V_{max}$ gets close to 35–45 kV (depending on the system). Fast wave power transfer increases when reducing the thickness of the evanescent layer $d_{evan}$ (the far SOL region between the antenna and the plasma where $n_e < n_{e\_CutOff}$); wave propagation in the plasma edge is also affected by density gradients because of a diffraction index mismatch effect. For a given edge gradient, it can be shown (see [2]) that the coupling resistance is expected to behave as:

$$R_c \propto \exp(-\alpha d_{evan}) \quad (2)$$

where $\alpha$ is a tunneling factor that depends on the specific antenna geometry. This was verified experimentally, for example on AUG [3] and Tore-Supra [4]. In ITER there are significant uncertainties in the density profiles predicted in the SOL, which lead to large uncertainties in the predicted coupled power (between 10 MW and 20 MW per antenna limited by the installed generator power) using antenna simulation codes [5] and taking into account the various operating limits in the antenna system (e.g. maximum voltage at the straps and in the transmission lines, radio-frequency (RF) field at the 3-port junction, etc) [6].

Some years ago, it was proposed to use local gas injection [7] as a tool to tailor the electron density in front of the ICRF antennas during the pulses and hence maximize or control the antenna coupling resistance. A similar technique is used to reduce the reflection coefficient of lower hybrid current drive (LHCD) antennas (see [8] and references therein). Experiments to assess the efficiency of this technique for ICRF heating have been performed under the coordination of the International Tokamak Physics Activity (ITPA) on ASDEX Upgrade (AUG) [9, 10], JET [11, 12], DIII-D [13, 14], Tore-Supra (summarized in [7]) and TEXTOR [15, 16]. This paper which concentrates on the recent experiments from AUG, JET and DIII-D, divertor devices of most relevance for ITER, summarizes these experiments, highlights the similarities or differences in the experimental results and describes the needs for modeling to assess the suitability of the location of ITER gas injection [17, 18] for the purpose of ICRF coupling enhancement.

The paper is organized as follows: in section 2 the machine parameters and experimental conditions are described for AUG, DIII-D, and JET. The JET experiments were performed with the ITER-Like Wall (ILW, tungsten divertor and beryllium wall). Section 3 describes the experimentally observed effects of local gas injection on the SOL density, antenna coupling and other plasma parameters. The mechanisms leading to the increase of the antenna coupling resistance are discussed in section 4. In support of the experimental measurements, plasma boundary modelling using the EDGE2D-EIRENE code (for JET and AUG) and the EMC3-EIRENE package (for AUG) has been attempted and the results are described. Concluding remarks and prospects for future work are offered in section 5.

## 2. Experimental setups

The main parameters of the AUG, JET and DIII-D experiments presented here are listed in table 1. The experiments were performed using central fast wave fundamental hydrogen minority (~5% hydrogen) heating in deuterium plasmas with $f_{ICRF}/B_T \sim 15$ MHz $T^{-1}$. On ITER ($f_{ICRF}$ in the range 40–55 MHz), this ICRF heating scenario could only be used at half field ($B_T = 2.65$ T). Although the reference scenarios for full field

**Table 1.** Tokamak and ICRF heating system parameters.

| | AUG | JET | DIII-D |
|---|---|---|---|
| ICRF system | Four 2-strap antennas (1, 2, 3, 4) with:<br>Antennas 1 & 3 (boron coated limiters) and 2 & 4 (W coated limiters) paired by 3 dB hybrid couplers. | Four 4-strap antennas (A, B, C, D) with:<br>– C and D paired by external conjugate T (ECT) junctions<br>– A and B paired by 3 dB hybrid couplers | Three 4-strap antennas (called 285/300, 0, and 180 antennas) |
| $f_{ICRF}$ | 30 or 36.5 MHz | 42 MHz | 60 and 90 MHz |
| $P_{ICRF}$ per antenna | 10 kW to 0.8 MW | <1 MW | 0.1 kW to 1 MW |
| Heating scheme | $N = 1$ (H)D minority | $N = 1$ (H)D minority | Electron landau damping/ transit time magnetic pumping |
| $k_{//,0}$ ($m^{-1}$) | 8 ($\pi$ phasing) | 6.6 ($\pi$ phasing) | 6 (285/300) & 7.4 (0, 180) ($\pi/2$ phasing) |
| $n_{e,cut\text{-}off}$ | $5 \times 10^{18}$ or $4 \times 10^{18}$ $m^{-3}$ | $2 \times 10^{18}$ $m^{-3}$ | $0.5 \times 10^{18}$ or $0.9 \times 10^{18}$ $m^{-3}$ |
| $d_{strap\text{-}separatrix}$ | 9–14 cm | 10–12 cm | 10–16 cm |
| $B_T/I_p$ | 2 T/0.8 MA or 2.5 T/0.8 MA | 2.7 T/2.5 MA | 1.3–1.9 T/1.3 MA |
| Plasma shape | Lower single null with cryo-pumped divertor | | Double null with cryo-pumped divertors |
| Other plasma heating | $P_{NBI} = 5$ MW<br>$P_{ECRH} = 1.3$ MW | $P_{NBI} = 13$–$15$ MW | $P_{NBI} = 6$–$8$ MW |
| Confinement regime | ELMy H-mode<br>$H_{98(y,2)} \approx 0.95$ | ELMy H-mode<br>$H_{98(y,2)} \approx 0.8$ | ELMy H-mode<br>$H_{98(y,2)} \approx 1$ |
| Local gas flow | 0.5–1 $\times 10^{22}$ el $s^{-1}$ | 0.5–2 $\times 10^{22}$ el $s^{-1}$ | 1.5 $\times 10^{22}$ el $s^{-1}$ |

ITER operation are 2nd harmonic tritium ($f_{ICRF}/B_T \sim 10$ MHz $T^{-1}$), fundamental $^3$He ($f_{ICRF}/B_T \sim 10$ MHz $T^{-1}$) or fundamental deuterium heating ($f_{ICRF}/B_T \sim 7.5$ MHz $T^{-1}$) [19], these experiments are relevant for ITER operation because the phenomenon involved in the increase of the antenna coupling resistance when using local gas injection are essentially related to SOL physics and magnetic field line geometry.

The geometry of the antennas, gas injection location and the lines of sight of the main diagnostics used in the experiments are shown in figures 1–3. Readers are invited to refer to these figures for the exact positions of antennas, gas inlets, diagnostics, etc, when following the description of the experiments. In all cases, divertor gas injection was toroidally distributed while outer mid-plane (OMP) and top injection were toroidally localized. On JET, at each toroidal location, top gas injection was poloidally distributed (see figure 2). We note that on JET the term GIM is used locally to denote 'Gas Injection Module' and will henceforth be used throughout this paper, specifically in the legends of several figures. All experiments were performed with Type I ELMy H-mode plasmas.

The effect of local deuterium injection was investigated by replacing the standard divertor injection by OMP or top injection (or adding localized midplane gas in the case of DIII-D), with otherwise fixed plasma parameters. The coupling resistance $R_c$ was evaluated using voltage and current probes in the transmission lines (AUG) or RF directional couplers (JET, DIII-D). Vacuum losses were accounted for. In these experiments, $R_c$ was monitored as a function of the gas injection location, at different gas rates and different distances between the separatrix and the antenna. For the analysis, the measurements of $R_c$ during ELMs were filtered out since the inter-ELM phases correspond to the lowest coupling resistance and maximum antenna voltages. The electron density $n_e$ was measured using mid-plane microwave reflectometers (AUG, JET, DIII-D), and Lithium beam diagnostics (AUG, JET). The effect of main chamber injection on other plasma parameters (impurity levels, confinement time, etc) was also monitored.

It is worth reporting some implementation and operational limitations encountered during these experiments: on AUG, a poloidally distributed gas inlet integrated in an antenna limiter was also tested [9]. At the highest gas rates (~$10^{22}$ el $s^{-1}$) however, the beneficial effect on antenna loading was hindered by an increased probability of arcing and a higher W sputtering yield at the limiter where the antenna valve was fitted. In this specific case, bringing the inlets outside the antenna box and retracting them radially could be an improvement. Gas fuelling must also be compatible with the operation of other systems and diagnostics; for example injecting gas too close from Li-beam diagnostics can compromise these measurements.

## 3. Experimental results

### *3.1. Effect of main chamber gas injection on ICRF antenna loading*

On JET, AUG and DIII-D, midplane gas injection leads to a substantial increase of the coupling resistance of the antennas located close to the gas injection point. Examples for AUG and JET are shown in figure 4. The differences in

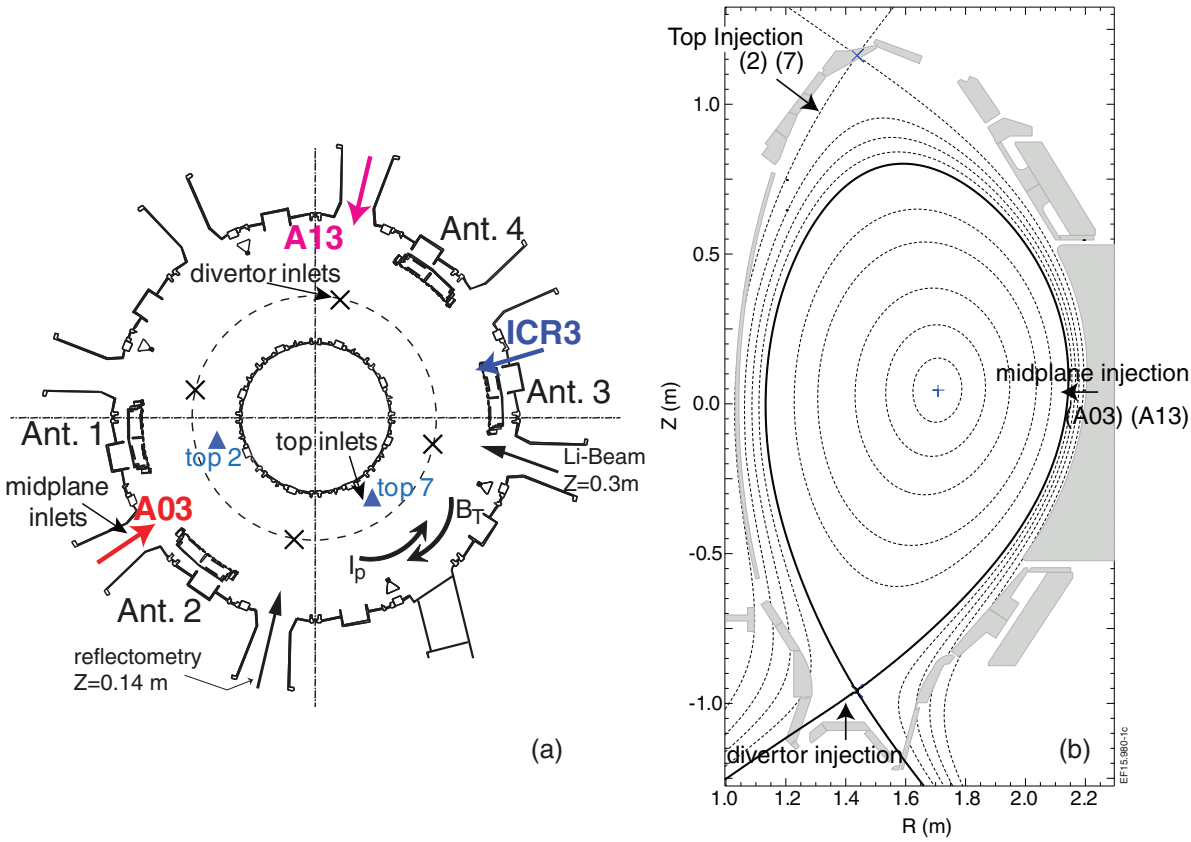


**Figure 1.** Top view (a) and poloidal cross-section (b) of AUG illustrating the position of the ICRF antennas and the location of the gas inlets. The SOL diagnostics lines of sight are also indicated.

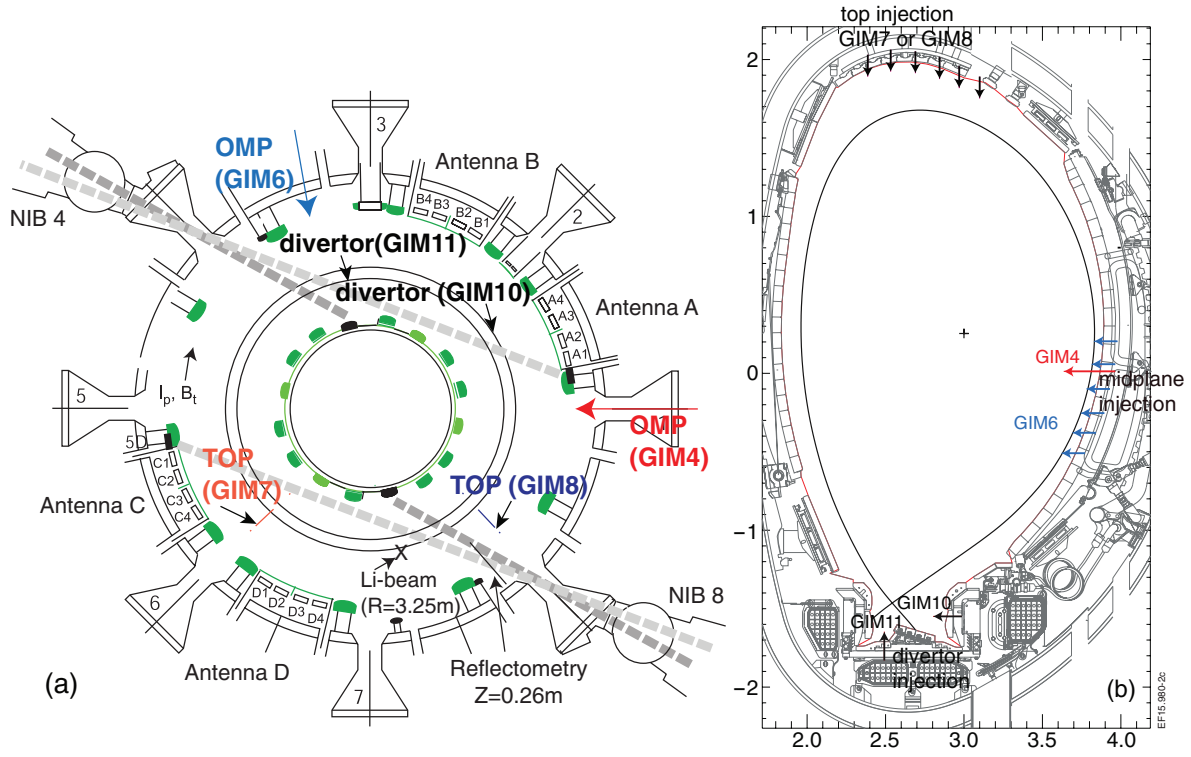


**Figure 2.** Top view (a) and poloidal cross-section (b) of JET illustrating the position of the ICRF antennas and the location of the gas inlets. At each toroidal location (GIM7 or GIM8) the top gas injection is poloidally distributed. The SOL diagnostics lines of sight are also indicated.

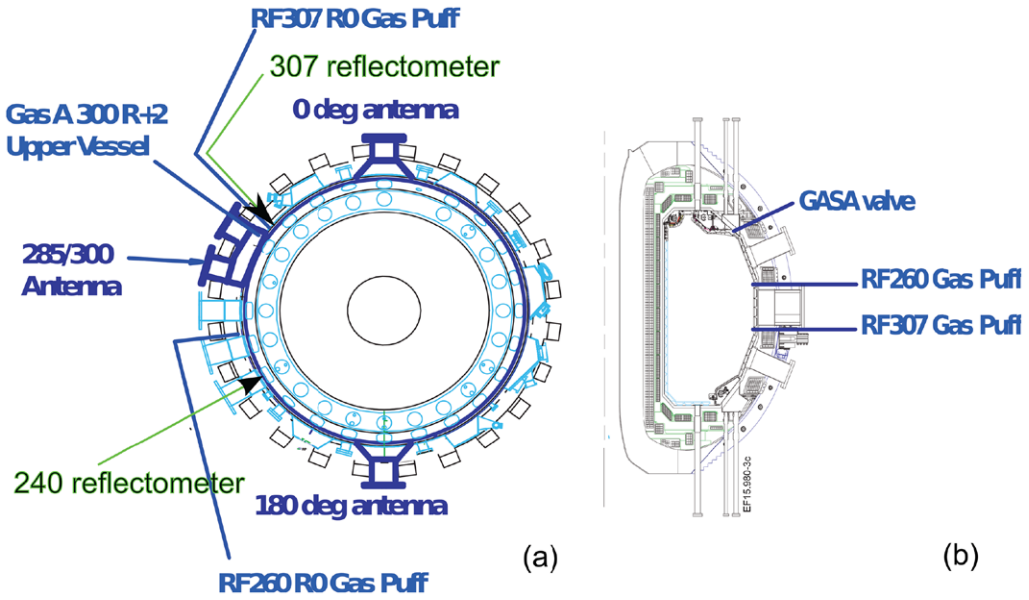


**Figure 3.** Top view (a) and poloidal cross-section (b) of DIII-D illustrating the position of the ICRF antennas and the location of the gas inlets. The SOL diagnostics lines of sight are also indicated.

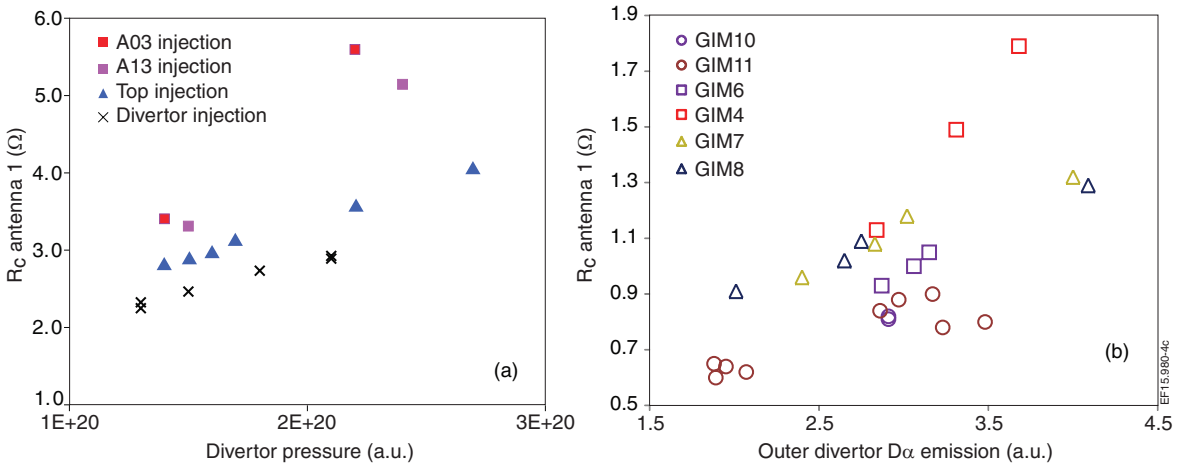


**Figure 4.** Antenna coupling resistance using divertor, outer mid-plane or top gas inlets (see figure 1 for exact locations). (a) AUG Antenna 1, Rc is plotted versus the sub-divertor pressure, injection rate is in the range 0.5–1.3 $\times$ $10^{22}$ el $s^{-1}$; $d_{\text{Antenna-LCFS}} = 5$ cm. (b) JET antenna A, $R_c$ is plotted versus the $D_\alpha$ emission intensity in the outer divertor, injection rate is in the range 0.5–1.7 $\times$ $10^{22}$ el $s^{-1}$; $d_{\text{Antenna-LCFS}} = 5.5$ cm.

net fueling efficiency of the different gas valves have been normalized using a proxy for the divertor neutral density: due to the divertor geometry, and positions of the divertor injection and pumping throats, the most meaningful renormalization is obtained using the sub-divertor pressure on AUG and the intensity of the $D_\alpha$ emission in the outer divertor on JET. On both machines, and for all gas inlets, $R_c$ increases when increasing the gas injection rate (and divertor neutral density), but in addition, antenna coupling resistance is maximized when using OMP gas injection close the active antenna(s).

In figure 5, the coupling improvement (relative to the coupling obtained with divertor gas injection with similar rate) when using midplane injection or toroidally localized top injection is plotted as a function of the gas valve—antenna toroidal distance. For OMP injection this is defined as the toroidal distance in meters at the radial position of the antenna. For top injection, the gas injection—antenna distance is the shortest distance along the torus surface. For OMP injection, the coupling improvement decreases exponentially with the gas inlet-antenna distance with a characteristic decay length of ~2 m on JET and ~4 m in AUG (figure 5) in these experimental conditions. Top gas injection leads to a (moderate) global improvement of the ICRF antennas loading, but no additional toroidally localized improvement is observed, even when the gas injection is magnetically connected to the antennas (see discussion in section 4.3).

On all three devices, a SOL density increase is observed when using mid-plane or top gas (but with smaller effect) injection. An example for DIII-D is shown in figure 6, where injecting ~2.6 $\times$ $10^{21}$ el $s^{-1}$ close to the 285/300 antenna and to the 307 deg. reflectometer leads to an outward shift of 1 cm of the cut-off layer and an increase in the antenna coupling resistance [14]. The strong oscillations in the edge density are due to ELMs in these ELMy H-mode discharges. Other

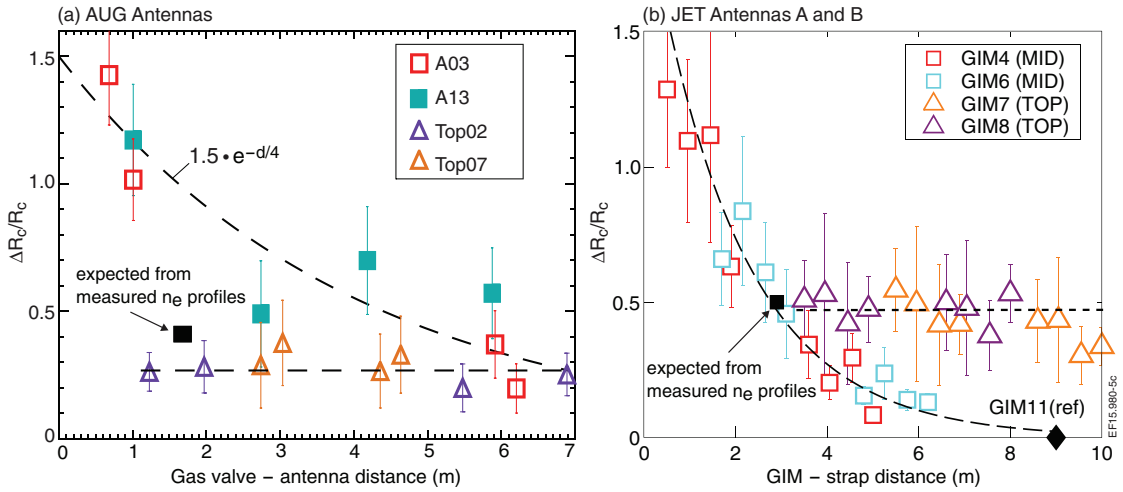


**Figure 5.** AUG (a) and JET (b), relative coupling resistance increase of the antenna straps w.r.t. divertor fuelled discharges plotted as a function of the injection-antenna distance. For AUG, the data-set includes the 4 antennas using A03, A13, Top2 and Top7 injection (see figure 1(a)) at rate ~1.2 × $10^{22}$ el $s^{-1}$. For JET, GIM 4, 6, 7 and 8 (see figure 1(b)) at rate (1.6–1.8) × $10^{22}$ el $s^{-1}$ were used. In (b), the black solid square is the coupling improvement expected from the simple 1D code using density profiles from reflectometry (see also figure 8). In this case, the toroidal distance between the reflectometer Line-of sight and the gas inlet (GIM4) is the abscissa.

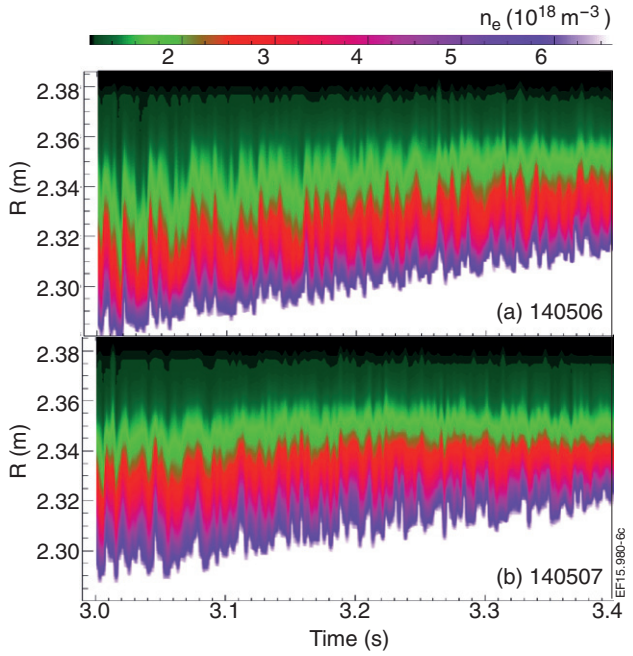


**Figure 6.** On DIII-D, density profiles measured at port 307deg., without (a) or with (b) 2.6 × $10^{21}$ el $s^{-1}$ injection from a local midplane valve (FW307 in figure 1(c)). In both discharges, the outer gap was ramped from 8 cm (3 s) to 3 cm (3.4 s) and the power applied to the 285/300 antenna was 0.1 kW.

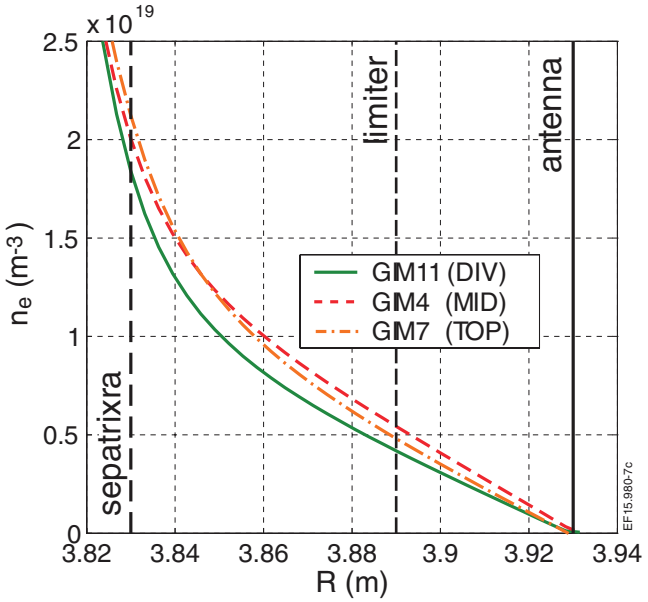


**Figure 7.** On JET, density profiles measured by reflectometry. Data are averaged over 1 s and ELMs are filtered out. The flow rates are GIM11: 1.85 × $10^{22}$ el $s^{-1}$; GIM4: 1.65 × $10^{22}$ el $s^{-1}$; GIM7: 1.6 × $10^{22}$ el $s^{-1}$.

examples of SOL density measurements when using OMP injection are shown on figures 7 (JET) and 12 (AUG). It is worth mentioning that in the AUG case, the measurements are performed when antenna 2, located toroidally 20 deg. from the reflectometer (see figure 1), is not powered (induced noise when nearby antenna is active).

The antenna coupling resistance increase was found quantitatively consistent with the SOL density measurements in DIII-D [14], and JET [11] when the toroidal distance between the gas injection and the location of SOL measurements coincides with the gas injection-antenna distance. On JET, a simple 1D fast wave propagation and coupling code [11] with the plasma $n_e$ profiles measured by the reflectometer (see figure 2 for reflectometer position) was used to estimate the coupling resistance. The results are shown in figure 8. A (unique) scaling factor was applied to the coupling resistance from the model to match the experimentally measured antenna-A coupling resistance when using divertor gas injection (module 11) with 1.8 × $10^{22}$ el $s^{-1}$. Highlighted in figure 8 is the 50% increase in coupling resistance expected from the density measurements (figure 7) and the coupling model when changing the gas injection from divertor (module 11) to OMP (module 4), if an A2 antenna was located in front of

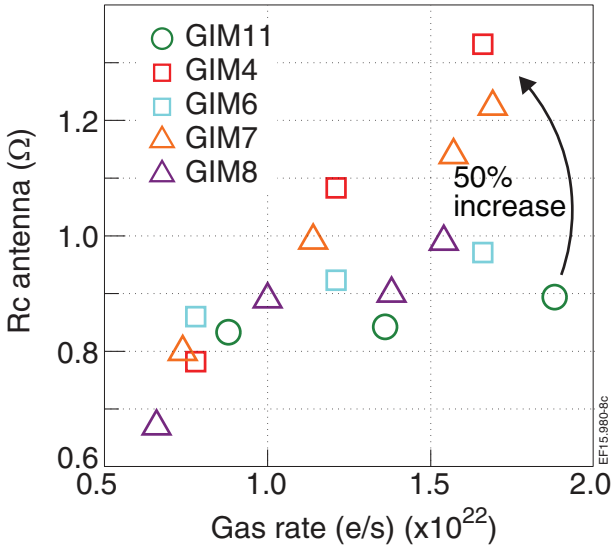


**Figure 8.** For JET, antenna coupling resistance calculated using a simple 1D coupling code with the density profiles from reflectometry as input. The points used to calculate the 'expected' coupling improvement at the reflectometry line of sight and reported in figure 5(b) are indicated with arrows.

the reflectometer line of sight. Taking into account the toroidal angle between the reflectometer and OMP gas injection location (module 4, which converts into 3 m toroidal distance for $R_{\mathrm{ant}} = 3.93$ m), this expected antenna coupling increase is marked by a solid black square in figure 5(b), and agrees well with the measured antenna coupling improvement when using OMP gas injection.

On AUG, two different approaches have be used to predict the expected coupling resistance increase from the measured density profiles when using OMP gas injection: (a) the same simple 1D antenna coupling model as just described together with reflectometry measurements; and (b) an extrapolation of the expected coupling improvement from the antenna '$R_{\mathrm{c}}$ experimental behavior' when moving the plasma outer radius. Both approaches gave the same result, the latter is described here: consistent with equation (2), the measured $R_{\mathrm{c}}$ during plasma outer radius scans using divertor gas injection can be fitted with an exponential of the form:

$$R_{\mathrm{c}} \propto R_{\mathrm{c},0} \mathrm{e}^{-\kappa(R_{\mathrm{ant}} - R_{\mathrm{CutOff}})}, \tag{3}$$

where $R_{\mathrm{ant}}$ and $R_{\mathrm{CutOff}}$ are the radial position of the antenna and cut-off layer respectively; $\kappa = 18\ \mathrm{m}^{-1}$ was fitted from the experimental data. From (3), the ~2 cm shift in the cut-off density radial position observed by the reflectometry when using OMP gas from A03 (figure 12) should lead to a 40% increase of $R_{\mathrm{c}}$ if the antenna was located at the reflectometer toroidal position, i.e. 1.75 m away from the gas injection point. The same value of 40% increase in $R_{\mathrm{c}}$ is obtained from the simple 1D coupling code using the measured density profiles. Both estimates are lower than the measured antenna $R_{\mathrm{c}}$ improvement during OMP gas injection (see figure 5(a)) even taking into account the experimental error bars. A possible explanation is that local modifications of the SOL density in front of the powered antenna (not captured by the currently available SOL measurements) are also occurring. In the next AUG campaign, the new 3 strap antenna [20] will be fitted with reflectometers which will allow measurement of the density directly in front of the antenna. This will hopefully shed some light on the possible density modifications driven by the ICRF power in front of the antennas (see also discussion in section 4.1).

### *3.2. Effect of main chamber gas injection on ICRF heating and plasma parameters*

A legitimate question related to the use of local gas to improve ICRF wave coupling is the impact of this technic on the plasma heating efficiency. Although the ICRF heating efficiency was not specifically evaluated in these experiments (for example using the Break-in Slope analysis technique as described in [21]) the plasma core kinetic profiles (Te and ne) are not modified whether divertor, top or OMP gas is used. This is illustrated for JET on figure 9, where the time trace of the electron temperature at the plasma centre, and electron plasma energy are plotted for a pulse with divertor gas injection and OMP injection respectively. The electron temperature and electron density profiles for these two pulses are plotted on figure 9(d). Profiles are taken before the sawtooth crashes; data are averaged over five time windows of 0.1 s each as shown in figure 9(c). In these plasma conditions, fast-wave heating results predominantly to an electron heating via slowing down of the fast H ions, with a typical centre electron temperature response of ~0.5 keV $\mathrm{MW}^{-1}$. The electron kinetic profiles overlay perfectly, suggesting that within measurement errors bars, the fast wave propagation and absorption characteristics are the same, independent of the gas injection location.

An important issue when considering gas injection from different locations is the consequence of using main chamber instead of divertor gas on plasma energy confinement: In JET and AUG, no degradation of pedestal pressure (see figure 9(d)) and confinement was observed when using the midplane or top inlets instead of the divertor inlets at the same gas fuelling level. An example for JET is shown in figure 10 where for a data-base of H-mode pulses, the $H$ factor $H_{98(y,2)}$ is plotted as a function of the $D_\alpha$ emission in the outer divertor (again to normalize for the differences in net fueling efficiency of the different gas valves). The quantity of gas required for antenna coupling improvement is also key, particularly since increasing gas dosing from the main chamber can have a negative impact on plasma energy confinement [22] in existing tokamaks. In this context it is important to emphasize that the antenna coupling improvements reported here are obtained when using moderate gas rates, and that this technique was used during the development of plasma scenarios in JET [23, 25]. For example on AUG and JET, the improvement in the antenna loading was ~50% when fuelling the plasma only with nearby midplane inlets instead of divertor inlets at an injection rate compatible with the development of plasma scenarios: During the experiments described here, the normalised confinement enhancement factor was $H_{98(y,2)} \approx 0.95$ with $0.75 \times 10^{22}$ el $\mathrm{s}^{-1}$ injection rate in AUG [9], and $H_{98(y,2)} \approx 0.8$ with $1.0 \times 10^{22}$ el $\mathrm{s}^{-1}$ in JET. It is worth mentioning that the $H$-factor in these JET experiments is in line with the JET-ILW

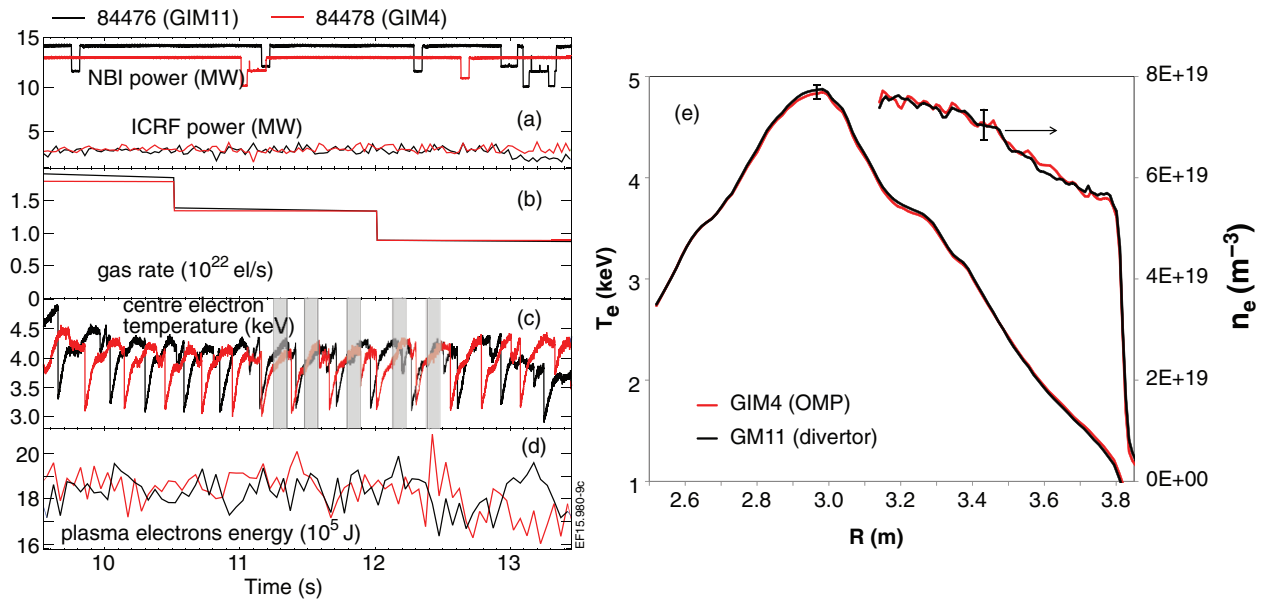


**Figure 9.** JET time traces and electron kinetic profiles when using divertor or OMP gas injection in JET. The time traces are (a) the auxiliary heating power, (b) the $D_2$ gas injection rate, (c) the electron temperature at the plasma centre, and (d) the total electron energy. Details of the Te (left *y*-axis) and ne (right *y*-axis) profiles are shown in (e). The profiles are averaged over the time intervals indicated in grey on the time trace graphs. Error bars correspond to the scattering in the data.

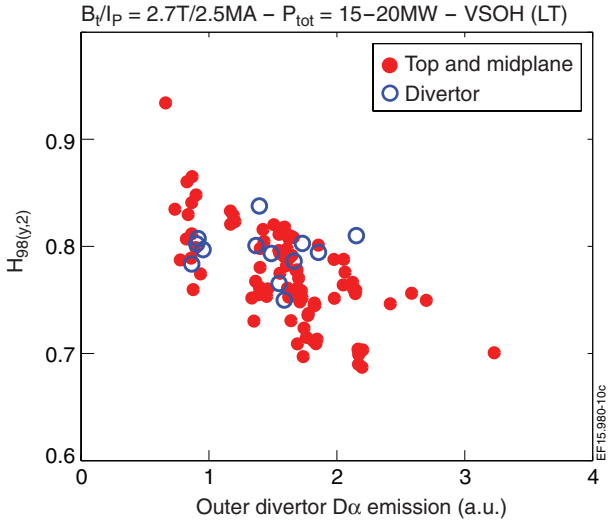


**Figure 10.** JET, $H_{98(y,2)}$ versus outer divertor $D_\alpha$ emission for a series of pulses with divertor or (midplane + top) gas injection. Injection rate is in the range $0.5 \times 10^{22}$–$2.7 \times 10^{22}$ el $s^{-1}$. This data-set fits in the JET-ILW confinement data-base (low triangularity baseline scenario) described in [24].

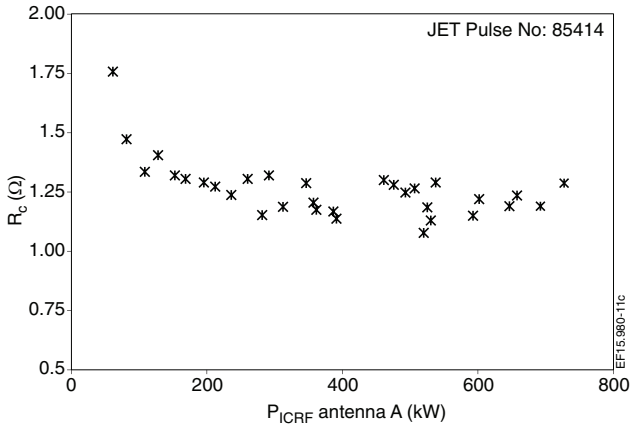


**Figure 11.** JET, pulse 85414. Coupling resistance of antenna A versus launched power. GIM4 injection rate is $4 \times 10^{21}$ el $s^{-1}$, and total injection rate from all gas injection modules is $1.7 \times 10^{22}$ el $s^{-1}$.

H-mode plasma database published in [24]. Understanding the modest confinement of JET-ILW plasma (compared to JET-C) is still the subject of active research [25]. In these ICRF coupling experiments the strike point position being located away from the divertor pumping throat was also unfavourable. Better performance (for a given gas load) is obtained when putting the strike point closer to the pumping throat [25].

Optimized gas injection was found to be beneficial for reducing the W sputtering at the AUG antenna limiters [9, 20], On JET, a reduction of the plasma W [11] or Ni [26] content at mid-radius was also observed when using midplane or top inlets during ICRF heating. There are several possible explanations for these observations: (a) increased coupling resistance leads to a reduction of the RF fields which drives the RF sheath rectification responsible for the ICRF specific impurity release [27]; (b) a reduction of the SOL plasma temperature close to the gas injection which reduces the tungsten sputtering yield [28]; (c) the somewhat higher ELM frequencies observed on JET with main chamber gas injection can also contribute to the lower levels of impurities measured when switching from divertor to main chamber injection [29].

## 4. Understanding the antenna coupling resistance improvement with local gas injection

### *4.1. Mechanisms leading to localized density increase*

Interaction of ICRF power with the SOL plasma has been observed experimentally on many tokamaks including AUG

**Table 2.** typical $E_{//}$ intensity in front of JET and AUG antennas.

| | JET | | AUG | |
|---|---|---|---|---|
| | $E_{//}$ intensity | $E_{//}/f_{ICRF}$ | $E_{//}$ intensity | $E_{//}/f_{ICRF}$ |
| $P_{ICRF} = 200$ kW per antenna | 3.75 kV m$^{-1}$ | 0.09 kV (m MHz)$^{-1}$ | 2.5 kVm$^{-1}$ | 0.065 kV (m MHz)$^{-1}$ |
| $P_{ICRF} = 800$ kW per antenna (recent JET coupling experiments described here) | 7.5 kV m$^{-1}$ | 0.19 kV (m MHz)$^{-1}$ | 5 kV m$^{-1}$ | 0.13 kV (m MHz)$^{-1}$ |

[28], JET [30], ALCATOR C-mod [31] and Tore-Supra [32]. Amongst the reported effects, RF sheaths rectification [27] is invoked to explain enhanced impurity production and local hot spots when using ICRF. The formation of RF induced flows in front of the powered antennas [33, 34], and ICRF power induced density depletion as observed in both JET and AUG [35] have also been reported. These local SOL plasma modifications in front of the antennas can contribute to the differences (on AUG) between the measured coupling resistance and the ones expected from the SOL measurements (performed away from the antennas) as described in section 3.1.

A natural question arises whether the coupling improvement when using gas injection close to the antenna is linked to the contribution (direct or indirect) of the ICRF power to gas ionization. For example, it was demonstrated that ICRF systems could be used to produce plasma of density ~$10^{17}$ m$^{-3}$ for tokamak wall conditioning on JET [36], AUG [37], TEXTOR [38] and Tore-Supra [39]. This process is called ion cyclotron wall conditioning (ICWC). These ICWC plasmas are usually performed with a tokamak toroidal field of few tesla. A working gas is $D_2$, $H_2$ or He with a neutral pressure in the range $10^{-5}$–$10^{-4}$ mbar. Plasma breakdown in these ICWC experiments is explained by the acceleration of electrons by $E_{//}$, the RF electric field in the toroidal direction generated by the antennas [36]. In this case, electrons gain energy up to few eVs (or few tens of eVs) where they can efficiently ionize the background gas. Theories have been developed to describe qualitatively the ICWC plasma formation [36], while more quantitative modelling requires codes to describe the acceleration of the electrons in the antenna electric field, and the electron-neutral and Coulomb collisions [40]. There are similarities between the ICWC experiments and the fast wave coupling experiments reported here, they are:

– Same antenna systems used in both experiments.
– In JET, when close OMP injection is used with an injection rate of ~$1 \times 10^{22}$ el s$^{-1}$, the neutral pressure measured in the vacuum transmission lines of the antennas (expected to be close to the pressure in front of the antenna) is in the same range as in the ICWC experiments (~$5 \times 10^{-5}$ mBar). This pressure drops by an order of magnitude when remote OMP injection is used.
– The maximum $E_{//}$ electric field as calculated by the antenna code TOPICA (Torino Politecnico Ion Cyclotron Antennas) [43], right in front of the antennas during the fast wave coupling experiments was typically in the range 7.5 kV m$^{-1}$ on JET and 5 kV m$^{-1}$ on AUG (corresponding to ~0.8 MW per antenna).

Hence specific experiments were conducted in AUG to investigate the effect of the RF power on antenna coupling. In particular the coupling resistance was measured in a large range of power (10 kW to 0.8 MW per antenna) with and without local gas injection. The results are reported in [9]: $R_c$ was found to decrease with increasing power for $P_{ICRF} < 20$ kW, and to be independent of the RF power above 50 kW. A very similar result for JET is shown for JET in figure 11; in this example plasma fueling is done using several main chamber GIMs (with the specific goal to increase the coupling resistance of all antennas) including the GIM 'GIM4' close to antenna A (GIM4 gas rate = $4 \times 10^{21}$ el s$^{-1}$). The behavior of $R_c$ at very low power could be interpreted in several ways: (a) the effect of RF power dissipation in the RF sheath rectification phenomenon [41]; (b) the effect of the ponderomotive force expelling the plasma in front of the antenna; (c) as tentatively proposed in [9], the effect of a very efficient absorption of the wave (for example via RF ionization) at low power which saturates above 10–20 kW. However (c) is unlikely because in our range of pressure and frequency, direct damping of the wave on neutral (collisional damping) does not dominate (quivering motion of electrons much smaller than collision mean free path). Rather, ionization induced by the RF power could only be explained by electron acceleration in front of the antennas up to energies for which they can efficiently ionize neutrals along the field lines. For example, via interaction of the electrons with the slow wave in the far SOL [42], via acceleration in the antenna field $E_{//}$ [36], or via the ponderomotive force. The slow wave with $|n_{//}| > 1$ $\left(n_{//} = \frac{k_{//}}{k_0}\right)$ could be excited by the antennas in far SOL regions where the electron density is $n_e < n_{e\_crit} \sim 4 \times 10^{16}$ m$^{-3}$ bounded by the lower hybrid resonance (LHR) [1]. Accuracy of the density measurements in the SOL does not allow good measurements in this range of density (especially in front of the antennas), but one cannot exclude excitation of the slow wave in a thin layer in the far SOL, and its interaction with plasma at the LHR. Regarding the interaction of electrons with the antenna field, combining the electrons acceleration in the RF electric field and the collisional ionization cross-section, Lyssovian and Schuller have expressed the ionization efficiency of the electrons as a function of $E_{//}/f_{ICRF}$ [36]; below 0.1 kV (m MHz)$^{-1}$, the electrons cannot be efficiently accelerated to ionize the background neutrals. The typical $E_{//}$ electric fields right in front of the antenna during our coupling experiments were calculated using the TOPICA [43] antenna code and are listed in table 2:

We can now formulate three strong arguments, based on the experiments that suggest that the ICRF power does not substantially contribute to the ionization of the neutral injected

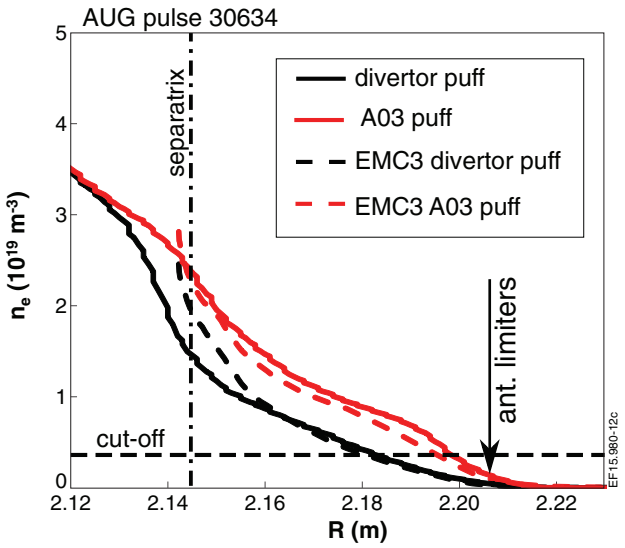


**Figure 12.** AUG SOL profiles measured by the reflectometer in sector 5 when using divertor (black) or sector 3 (A03) OMP gas puff (red). The profiles are averaged over a 0.2 s period at 2.2 s (divertor injection) and 6.0 s (A03 OMP injection). Profiles during ELM events were filtered out. Broken lines: EMC3-EIRENE simulations at the reflectometer line of sight when using divertor or OMP A03 gas injection. EMC3 simulations parameters were adjusted to fit Li-beam and divertor plasma measurements for pulse 31 269 with divertor gas injection.

close to the antennas and the local build-up of the density in the fast wave coupling experiments:

– The first argument is about the ICRF power for which fast wave coupling improvement was observed during local gas injection experiments; the effects of OMP gas injection on antenna loading is reproduced for a large range of antenna power in different machines: a few hundred watts to 1 MW in DIII-D, 10 kW to 1 MW in AUG, and in the MW range in JET. Should the RF power contribute significantly to the ionization of the gas in front of the antenna, a strong dependence with ICRF power is expected applying the qualitative Lyssoivan/Schuller criteria to our range of experimental conditions (see table 2).
– The second argument is related to the SOL measurements. Unfortunately measurements of the SOL density directly in front of the antenna or at locations magnetically connected to the antennas were not available during fast wave coupling experiments with local gas injection. But when such measurements could be performed (unfortunately with remote gas injection), instead of an increase, a depletion of the SOL density in a layer of few cm in front of the powered antennas is systematically observed [35]. In contrast, when these SOL measurements are connected to the LHCD launcher, a density increase in a few cm layer in front of the launcher could be observed when the LHCD power is applied [44]. We should also mention that some Langmuir probe measurements reported an 'effective' increase of the electron temperature on Tore-Supra when the probes were connected to active ICRF antennas [45]. These measurements were interpreted as a distortion of the *I–V* characteristic of the probe due to RF-sheath rectification.
– Finally, we emphasize again that the AUG density measurements shown in figure 12, are performed when antenna 2 (located toroidally 20 deg. from the reflectometer) is not powered. Therefore the measured density increase when using local gas in AUG can be attributed to the ionization of the gas by the plasma only.

To summarize this section, we repeat that antenna-plasma interactions are complex phenomena that are the subject of active research. Modelling of the possible role of the ICRF power on the SOL ionization was proposed in [51] and will be reported in the future. If specific ICRF wave-SOL interaction effects can change the density in front of the powered antennas, which is expected to impact the loading of the antennas, experimental facts suggest that the beneficial effect of local gas injection on antenna coupling derives essentially from the ionization of the neutrals by the plasma and subsequent local increase of the density in the SOL. In the next section, the modelling performed to describe ionization of the injected gas by the plasma is discussed.

### 4.2. SOL modelling

Preliminary modelling of the JET [46] and AUG experiments has been performed using the EDGE2D-Eirene code package which couples the 2D plasma fluid code EDGE2D [47] with the kinetic neutral Monte–Carlo code Eirene [48]. No ICRF wave plasma interaction effects are included in these simulations. The simulations are performed in the usual way, adjusting transport parameters (notably $D_\perp$) to match SOL profiles, in the case of discharges with gas puffing from the divertor. Then, switching the gas source position from divertor to OMP or top does show a density increase at the OMP but the magnitude of the SOL density increase cannot be quantitatively matched. For example on JET, the predicted shift in cut-off layer position (~2 mm) is much smaller than experimentally observed via density measurements and from antenna coupling analysis (see section 3.1). The main limitation is the 2D nature of the EDGE-2D code; in particular in the case of localized OMP injection, the neutral pressure and ionization source close to the injection point is underestimated (assumed uniform in the toroidal direction in the simulation).

A more realistic simulation must include 3D effects and this has started for AUG [49] using the EMC3-Eirene code package, where EMC3 is an edge 3D Monte Carlo plasma fluid code [50]. A comprehensive description of these EMC3 simulations for the AUG experiment is reported in a separate paper [51]. The AUG geometry is fully described in the code, in particular the toroidally non-axisymmetric nature of the plasma facing components, and the 3D location of the gas valves. Again, no ICRF wave plasma interaction effects are included in these simulations. As in the EDGE2D-Eirene simulations, first the particle transport and energy transport coefficients are adjusted for the case of divertor gas injection, to provide the best match to the corresponding measured plasma edge and SOL density and temperature at the outer midplane

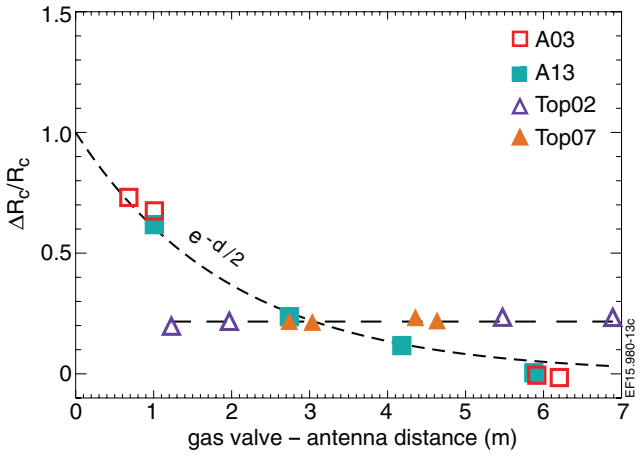


**Figure 13.** AUG, EMC3-EIRENE + felice calculation of the relative coupling resistance increase of the antennas w.r.t. divertor fuelled discharges plotted as a function of the injection-antenna distance. Figure reproduced with permission from [52, 53].

(SOL parameters measured by edge Thomson scattering and Li-beam diagnostic) and at the strike point (divertor probes saturation current). For all the measurements, ELMs were filtered out, so the modelling applies only to the inter-ELM periods. Then the only parameter changed in the simulations is the gas injection location; injection is switched to a toroidally localized OMP gas source or top source. In common with the experiment, top injection leads to an increase in the SOL density at the OMP (~5 mm shift of the cut-off), but it is not toroidally localized; this is a consequence of the toroidal spreading of the field lines in this magnetic configuration as explained in section 4.3. OMP gas injection leads to an asymmetrical large density increase in the midplane; maximum density increase is toroidally localized close to the gas injection location, in line with the experimental findings. An example of an EMC3 simulation with OMP injection is shown in figure 12. The EMC3 density profiles are plotted at the reflectometer location using $1.2 \times 10^{22}$ el $s^{-1}$ gas from divertor or the OMP A03 valve located ~45 deg. toroidally from the reflectometer. In the simulations, the cut-off density at the reflectometer is shifted by ~2 cm when using A03 OMP gas puff which is in agreement with the measurements in similar conditions.

Further, the density profiles from EMC3 simulations were averaged poloidally and toroidally in front of the antennas. Then the antenna coupling resistance was computed using the fast wave coupling code FELICE [53]. The results extracted from references [51, 52] are presented in figure 13. Quantitatively, there are some differences between the modelling and the measurements for OMP injection; for example the exact amplitude of the $R_c$ increase for short gas-antenna distance, or the decay length of the coupling improvement versus distance. Several reasons could be invoked to explain these differences.

– The antenna response to inhomogeneous toroidally and poloidally density profiles might not be best captured by the profiles spatial averaging technique adopted in the analysis.
– ELMs were filtered out in the measurements used to constraint the EMC3-EIRENE modeling. However, the ELMs could change the SOL properties, and contribute to the ionization of the gas. In the next AUG experimental campaign, it is planned to reproduce these experiments and get new measurements in L-mode.
– As discussed in 4.1, ICRF wave-SOL interaction effects can change the density in front of the powered antennas.

However the qualitative (and to a first order quantitative) agreement between the 3D SOL modeling and the AUG experiments using local gas injection, gives confidence that EMC3-EIRENE modelling can adequately describe the effect of local gas puffing on the ICRF antenna coupling. More work is planned to benchmark the modelling against AUG and JET experiments so that future quantitative studies for ITER can be made with confidence: Some L-mode experiments are planned in AUG, and an EMC3-EIRENE model of JET relevant to these experiments will be developed.

### *4.3. Effect of field line topology on SOL density modifications during OMP and top gas injection and implications for ITER*

As described in the previous section, 3D SOL modelling renders the effect of rapid plasma transport along magnetic field lines and cross-field particle transport in the SOL, coupled with the localized nature of the injection and explains the asymmetrical density build-up at the OMP where the antennas are located. In this section, using 3D field line tracing, we explain qualitatively why both on AUG and JET, experiments with top gas injection did not lead to an increase of antenna coupling resistance. These qualitative arguments confirm the 3D SOL modeling for AUG (see section 4.2) and allow to discuss the merit of the proposed gas location that could be used to enhance ICRF antenna coupling on ITER.

When using OMP or top gas injection, the injected neutrals diffuse until they reach the plasma where they are ionized via electron impact. For the SOL conditions in AUG or JET the ionization distance is few tens of centimeters as is show by EDGE-2D (JET, AUG) and EMC3 modelling (AUG) [51]. Because of the predominant plasma transport along the field lines, the SOL density is expected to be at least partially toroidally asymmetric, when using toroidally localized gas injection, as was the case for OMP and top gas injection.

This in indeed verified in the case of OMP injection close to an antenna, gas ionization occurs at a short distance from the antenna (or directly in front of the antenna). For most of the magnetic field line configurations, the antenna is magnetically connected to the ionization source, or at a short distance from field lines connecting to the ionization source; hence the electron density in front of the antenna is increased.

In the case of toroidally localized top gas injection, both on AUG and JET, a global and moderate increase of the SOL density and antenna coupling resistance was observed experimentally, but the effect was spread more evenly in the toroidal direction: $R_c$ was slightly increased for all antennas around the torus. This can be qualitatively understood on the basis of magnetic field line geometry and is illustrated for JET and

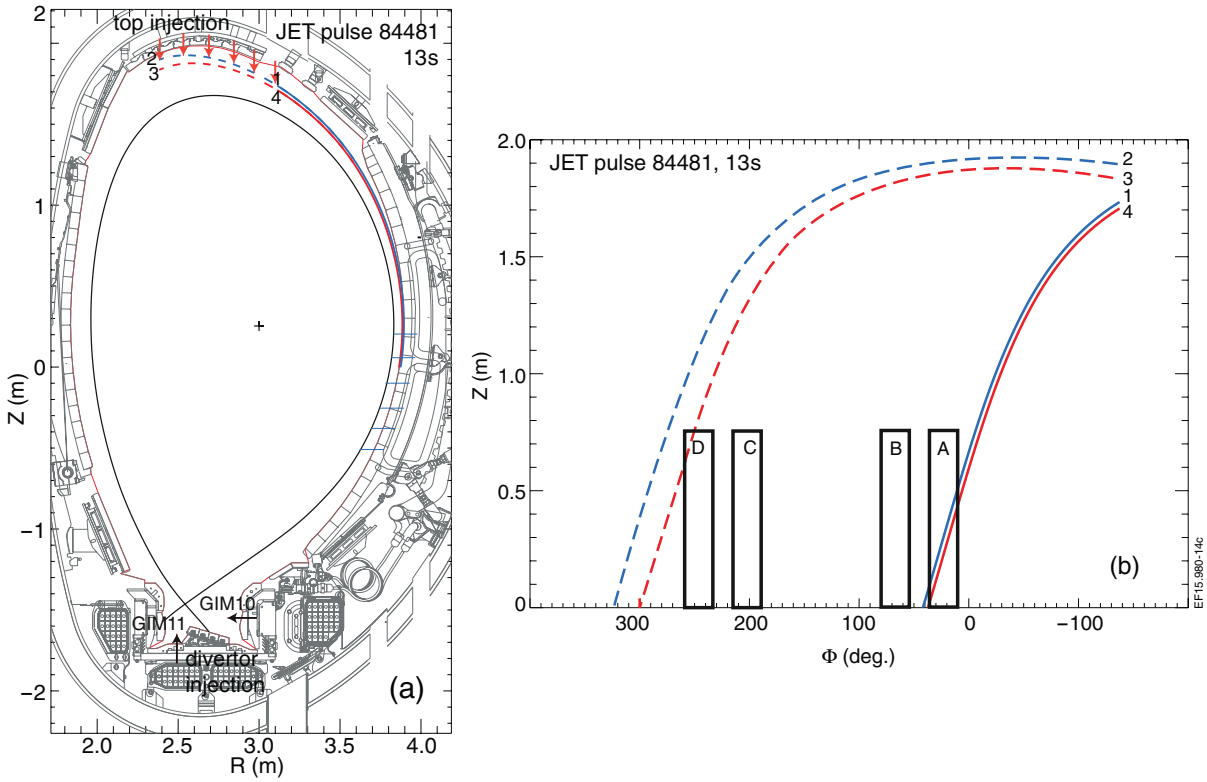


**Figure 14.** For JET, (a) poloidal cross sections showing the location of gas injection at one top toroidal location (GIM7) and field lines starting from the top of the plasma; (b) Field lines in the ($\Phi$, $Z$) plane (looking from the plasma). Field lines (starting points 1, 2, 3, 4) are mapped to $R = 3.885$ m and $R = 3.895$ m at the plasma midplane (cut-off location $\pm 0.5$ cm).

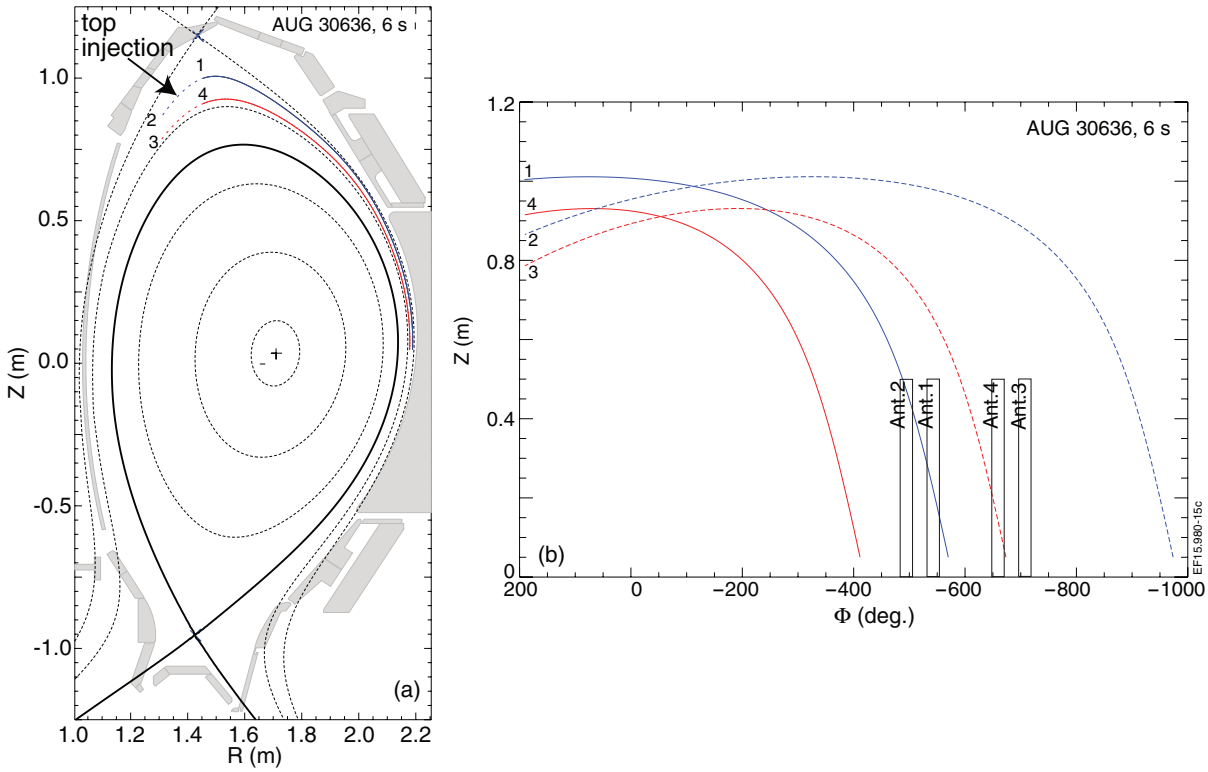


**Figure 15.** For AUG, (a) poloidal cross sections showing the location of gas injection at one top toroidal location (Top2) and field lines starting from the top of the plasma; (b) Field lines in the ($\Phi$, $Z$) plane (looking from the plasma). Field lines (starting points 1, 2, 3, 4) are mapped to $R = 2.18$ m and $R = 2.19$ m at the plasma midplane (cut-off location $\pm 0.5$ cm).

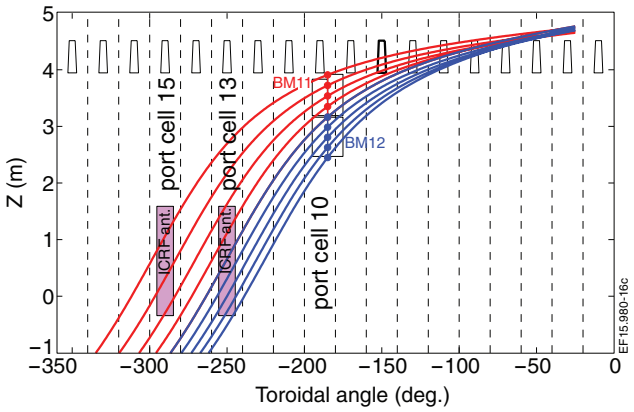


**Figure 16.** For ITER, example of field lines starting next to the blanket modules 11 (red) and 12 (blue) in port cell 10. Plasma parameters are for the $Q_{DT} = 10$ 15 MA reference scenario.

AUG in figures 14 and 15 respectively. Field line tracing in the magnetic equilibria used in the experiments shows how a density increase occurring on field lines at the top of the plasma spreads significantly in the toroidal direction at the midplane. In these plots field lines start from one toroidal position at the top of the machines, corresponding to the injection locations. The radial distance between the chosen field lines is 1 cm at the OMP, Field lines are evenly positioned around the cut-off.

In the JET case (figure 14), the poloidal distance between the starting points of the field lines corresponds to the poloidal extent of the top gas injection. In this case, most of the toroidal spread encountered when the field lines run from top injection towards the OMP, is explained by the poloidally distributed top gas injection. This can be seen from the ~250 deg. toroidal difference at $Z \sim 0$ between field lines 1/4 and 2/3 (figure 14).

For AUG where top injection is from a single point (figure 15), the poloidal range for the starting points of the field lines is chosen to correspond with the extent of the SOL region with enhanced density when using top injection (as obtained from SOL modeling i.e. [51]). In the AUG experiments, the higher upper plasma triangularity leads to a secondary $x$-point at the top of the machine (see figure 15) and the associated magnetic shear explains a large part of the toroidal spread encountered by field lines starting close to the top injection point (~300 deg. toroidal difference between line 2 and line 3 at $Z \sim 0$ in figure 15). The high field side position of the AUG top injection is also unfavorable for establishing a localized connection along field lines to the OMP (distance between line 2 and line 3 compared to distance between line 1 and line 4 at midplane).

On ITER, main chamber gas injection will be from the top, low field side [17]. Injection piping will be routed through the upper port plugs and gas will be puffed into a space between the shield blocks and water cooling manifolds, from where it will diffuse out into the main chamber through the gaps (~20 mm wide) between blanket modules (BM). The entry location cannot be precisely controlled since gas diffuses in the interspaces, but it is expected to spread poloidally roughly over the extent of BM11 and BM12 (see figure 16) and toroidally perhaps over the extent of a single BM (corresponding approximately to a toroidal angle of 10°). Figure 16 shows how the ITER ICRF antennas will be located in the OMP of port cells (PC) 13 and 15 and how field lines originating at different poloidal locations on BM11, and BM12 for gas injection from PC 10 will connect to the antennas for the baseline $Q_{DT} = 10$ equilibrium. On the basis of the results presented here, which show that some gain in coupling resistance is possible from localized top injection, ITER's gas injection system should allow some benefit for ICRF coupling. It will only be possible, however, to assess quantitatively the potential gain through predictive simulations for ITER. This in turn can be credible only if results from the experiments, can be satisfactorily modelled by 3D SOL modelling codes.

## 5. Conclusions and prospects

The experiments coordinated by the ITPA in AUG, JET and DIII-D have demonstrated that OMP gas injection strongly enhances the coupling resistance of nearby ICRF antennas. The effect is substantial at moderate gas rates (~$10^{22}$ el $s^{-1}$) that are compatible with the development of high performance scenarios. ICRH plasma heating and confinement properties are not affected when using OMP injection, while the core high-$Z$ core impurity content is slightly reduced.

On JET and DIII-D, the increase in SOL density observed with main chamber puffing is consistent with the increased antenna coupling resistance provided that the distance between the measurement line of sight and the injection location is taken into account. On AUG, the measured antenna coupling resistance improvement is larger than expected from SOL measurements, suggesting that local SOL modifications in front of the antennas also take place. However, the beneficial effect of local gas injection on antenna coupling is observed for a large range of ICRF power, and it appears it derives principally from the ionization of the neutrals by the plasma and subsequent local increase of the density in the SOL.

SOL modelling of the plasma-gas interaction has started on AUG using the 3D SOL modeling code EMC3-EIRENE. The strong localized increase of the SOL density close to the outer-midplane injection port and the beneficial effect on the loading of nearby antennas could be reproduced. As in the experiment, top gas injection leads to a global density increase in the OMP with a smaller and uniform (for all the antennas around the torus) increase in the antenna coupling resistance. This latter result is explained in terms of the specific plasma configuration (secondary $x$-point) in the AUG experiment. In JET, the geometry of the gas inlets (top gas injection poloidally distributed in JET) is responsible for the top injection results.

In this respect the location of the planned ITER gas injection system is favorable, but more simulation and experimental work is needed to quantitatively assess the capability of top low field side injection to increase the density in front of the ITER ICRF antennas. Experiments are planned in AUG and JET in 2016. In particular in AUG, new reflectometers will allow measurement of the density directly in front of some antennas, and injection from a gas inlet located at the top of the machine, on the low field side, closer to the ITER situation, will be tested. The simulations must involve 3D SOL codes to properly describe the toroidally localized ionization

sources and the magnetic field line topology. Benchmarking of the code against today's experiments must be performed before any application to ITER can be made with confidence.

## Acknowledgments

Careful review and suggestions from the referees is acknowledged. The views and opinions expressed herein do not necessarily reflect those of the ITER Organization or of the European Commission. This work has been carried out within the framework of the EUROfusion Consortium and has received funding from the Euratom research and training programme 2014–2018 under grant agreement No 633053. The views and opinions expressed herein do not necessarily reflect those of the European Commission. This work was also part-funded by the RCUK Energy Programme under grant EP/I501045.

## References

[1] Stix T.H. 1992 *Waves in Plasmas* (New York: AIP) ISBN 0-88318-859-7
[2] Bilato R., Brambilla M., Hartmann D.A. and Parisot A. 2005 *Nucl. Fusion* **45** L5–7
[3] Bobkov V. *et al* 2006 *Nucl. Fusion* **46** S469–75
[4] Clairet F., Colas L., Heuraux S. and Lombard G. 2004 *Plasma Phys. Control. Fusion* **46** 1567–80
[5] Messiaen A. *et al* 2010 *Nucl. Fusion* **50** 025026
[6] Durodié F. *et al* 2014 *Phys. Plasmas* **21** 061512
[7] Mayoral M.-L. *et al* 2010 *Fusion Energy* (*Proc. 23rd Int. Conf. Daejeon*) (Vienna: IAEA) CD-ROM file [P1-11] and www-naweb.iaea.org/napc/physics/FEC/FEC2010/index.htm
[8] Ekedahl A. *et al* 2012 *Plasma Phys. Control. Fusion* **54** 074004
[9] Bobkov V. *et al* 2014 *AIP Conf. Proc.* **1580** 271
[10] Jacquet P. *et al* 2012 *Nucl. Fusion* **52** 042002
[11] Lerche E. *et al* 2015 *J. Nucl. Mater.* **463** 634–9
[12] Mayoral M.-L. *et al* 2007 *AIP Conf. Proc.* **933** 55
[13] Pinsker R.I. *et al* 2010 *37th EPS Conf.* http://ocs.ciemat.es/EPS2010PAP/pdf/O4.124.pdf
[14] Pinsker R.I. *et al* 2011 *AIP Conf. Proc.* **1406** 313
[15] Van Wassenhove G. *et al* 2011 *Proc. 38th EPS Conf. on Plasma Physics ECA* vol 35G, P5.098
[16] Stepanov I. *et al* 2011 *AIP Conf. Proc.* **1406** 85
[17] Maruyama S. *et al* 2010 *Fusion Energy* (*Proc. 23rd Int. Conf. Daejeon*) (Vienna: IAEA) CD-ROM file [P5-24] and www-naweb.iaea.org/napc/physics/FEC/FEC2010/index.htm
[18] Maruyama S. *et al* 2012 *Proc. 24th Int. Conf. on Fusion Energy* (*San Diego*) ITR/P5-24
[19] Lamalle P. *et al* 2009 *AIP Conf. Proc.* **1187** 265
[20] Bobkov V. *et al* 2013 *Nucl. Fusion* **53** 093018
[21] Lerche E.A. *et al* 2008 *Plasma Phys. Control. Fusion* **50** 035003
[22] Saibene G. *et al* 1999 *Nucl. Fusion* **39** 1133–56
[23] Giroud C. *et al* 2014 Towards baseline operation integrating ITER-relevant core and edge plasma within the constraint of the ITER-like Wall at JET *Proc. of the 25th IAEA Fusion Energy Conf. 2014* (*Saint Petersburg, Russia 13–18 Oct. 2014*) EX/P5-25 http://www-naweb.iaea.org/napc/physics/FEC/FEC2014/fec_sourcebook_online.pdf
[24] Beurskens M.N.A. *et al* 2014 *Nucl. Fusion* **54** 043001
[25] Nunes I. *et al* 2014 Compatibility of high performance operation with JET ILW [EX/9-2] *Paper presented at 25th IAEA Int. Conf. on Fusion Energy* (*St Petersburg*)
[26] Czarnecka A. *et al* 2012 *Plasma Phys. Control. Fusion* **54** 074013
[27] Perkins F.W. *et al* 1989 *Nucl. Fusion* **29** 583–92
[28] Bobkov V. *et al* 2010 *Nucl. Fusion* **50** 035004
[29] Dux R. *et al* 2009 *J. Nucl. Mater.* **390–1** 858–63
[30] Klepper C. *et al* 2013 *J. Nucl. Mater.* **438** S594–8
[31] Wukitch S.J. *et al* 2007 *J. Nucl. Mater.* **363–5** 491–7
[32] Colas L. *et al* 2003 *Nucl. Fusion* **43** 1–15
[33] Becoulet M. *et al* 2002 *Phys. Plasmas* **9** 2619–32
[34] Van Eester D., Crombe K. and Kyrytsya V. 2013 *Plasma Phys. Control. Fusion* **55** 025002
[35] Colas L. *et al* 2015 *J. Nucl. Mater.* **463** 735–8
[36] Lyssoivan A. *et al* 2012 *Plasma Phys. Control. Fusion* **54** 074014
[37] Lyssoivan A. *et al* 2005 *J. Nucl. Mater.* **337–9** 456–60
[38] Esser H.G. *et al* 1997 *J. Nucl. Mater.* **241–3** 861–6
[39] Gauthier E. *et al* 1997 *J. Nucl. Mater.* **241–3** 553–8
[40] Tripsky M. *et al* 2014 *41st Conf. Plasma Physics (Berlin, 23–27 June 2014)* P1.133
[41] D'Ippolito D.A. and Myra J.R. 1996 *Phys. Plasmas* **3** 420
[42] Lyssoivan A. *et al* 2014 *41st EPS Conf.* http://ocs.ciemat.es/EPS2014PAP/pdf/P2.030.pdf
[43] Milanesio D., Meneghini O., Lancellotti V., Maggiora R. and Vecchi G. 2009 *Nucl. Fusion* **49** 115019
[44] Kirov K. *et al* 2013 *Plasma Phys. Control. Fusion* **55** 115008
[45] Colas L. *et al* 2007 *J. Nucl. Mater.* **363–5** 555–9
[46] Petrzilka V. *et al* 2012 *39th EPS Conf. on Plasma Physics* P2.027
[47] Simonini R. *et al* 1994 *Contrib. Plasma Phys.* **34** 368
[48] Wiesen S. www.eirene.de/e2deir_report_30jun06.pdf
[49] Zhang W. *et al* 2015 *AIP Conf. Proc.* **1689** 050006
[50] Feng Y. *et al* 2004 *Contrib. Plasma Phys.* **44** 57–69
[51] Zhang W. *et al* 2016 3D simulations of gas puff effects on edge density and ICRF coupling in ASDEX Upgrade *Nucl. Fusion* **56** 036007
[52] Bobkov V. *et al* 2015 *AIP Conf. Proc.* **1689** 030004
[53] Brambilla M. 1995 *Nucl. Fusion* **35** 1265–80
[54] Romanelli F. *et al* 2014 *Proc. of the 25th IAEA Fusion Energy Conf. 2014* (*Saint Petersburg, Russia 13–18 Oct. 2014*)